GeoScienceWorld
Lithosphere
Volume 2023, Article ID 5668451, 19 pages
https://doi.org/10.2113/2023/5668451

Lithosphere

Research Article

Study on Stress-Type Rockburst Mechanism Based on Continuous-Discontinuous Element Method

Kezhu Chen,[1,2] Tianbin Li,[1] Meiben Gao,[1,3] Chunchi Ma,[1] and Yan Zhang[1]

[1]*State Key Laboratory of Geohazard Prevention and Geoenvironment Protection, Chengdu University of Technology, Sichuan 610059, China*
[2]*Sichuan Communication Surveying & Design Institute Co., Ltd, Sichuan 610031, China*
[3]*School of Emergency Management, Xihua University, Sichuan 610039, China*

Correspondence should be addressed to Tianbin Li; ltb@cdut.edu.cn

Received 20 July 2022; Revised 30 January 2023; Accepted 11 February 2023; Published 8 May 2023

Academic Editor: Qian Liu

Rockburst plays a serious threat to personnel and equipment during underground engineering construction. The study of the rockburst mechanism is helpful to its prediction and prevention. Based on the characteristic analysis of a large number of rockburst cases, Li et al. proposed three stress-type and three stress-structural rockbursts and obtained the geological characteristics and occurrence criteria of these rockbursts, but the evolution process of rockbursts is still unclear. Based on the continuous-discontinuous element method, the characteristics of failure process, surrounding rock stress, motion, and energy of three stress-rockburst blocks are analyzed. The results show that rockburst failure generally goes through several stages, such as a few surfaces tensile failure, shallow shear failure, deep extension of tensile failure, shear failure communication, and rockburst occurrence. The total volume of rockburst blocks and the main distribution intervals of block diameters for different types of rockbursts are quite different, which are mainly affected by stress state and geological structure. The ejection velocity of the small block is always higher than that of the large block during the same one rockburst simulation, and the ejection velocity of the small block is from the surface. In the process of rockburst, not only the elastic strain energy is released but also the elastic strain energy is accumulated. The greater the rockburst intensity, the more the elastic strain energy is released, and the steeper the prepeak curve of elastic strain energy. The research results provide a reference for further understanding the mechanism of rockburst and lay a theoretical basis for the prevention and control of rockburst in underground engineering.

1. Introduction

With the development of society and economy, the earth surface resources can hardly meet the current development needs. People began to seek the necessary resources in the deep earth [1]. Apart from energy and minerals, a large number of underground spaces have gradually become the object of development and utilization, with an increasing number of long-buried tunnels [2]. However, with the increase in depth, the geological environment in which the rock mass exists is more complicated, and the in situ stress is higher. The geological disasters represented by rockburst will become more prominent, and their occurrence intensity and frequency of rockburst show an upward trend [3, 4]. From the location of rockburst occurrence, rockburst is widely distributed around the world [5]. The countries which, for some time, have been facing the problem of excavation-induced rockburst include South Africa, China, the United States, Canada, Norway, the Czech Republic, Poland, Russia, Sweden, Switzerland, and Korea, and this is not an exhaustive list, such as Altenberg tin mine in Germany, Leipzig coal mine in the United Kingdom, Falconbridge Nickel mine in Canada, Kolar gold mine in India, East Rand Proprietary Mines (ERPM) mine in South Africa, Idaho Lead-zinc-silver mine in the United States, Vietas hydropower diversion tunnel in Sweden, Kwanetsu tunnel in Japan, Heggure road tunnel in Norway, and so on, all have suffered rockburst. The occurrence of rockburst

is very sudden, random, and destructive, which seriously threaten the safety of construction personnel, equipment, and property [5–8]. It has caused huge losses to people's lives and property and brought unprecedented challenges to underground engineering design, construction, and production. Therefore, it is of great engineering value and theoretical significance to study the rockburst mechanism and know the breeding law of rockburst to ensure the safe construction of underground engineering, disaster prevention and mitigation, and emergency treatment.

Therefore, based on rockburst field examples [6, 7], a large number of scholars have studied the occurrence mechanism of rockburst from the perspectives of theory, rock mechanics test, and numerical simulation [8–12]. For example, Feng et al. [13] study the rockburst instability mechanism of entry floor-induced mining by considering the results from a laboratory test, numerical simulations, and field practice. Using years of theoretical studies and engineering practices, Cai et al. [14, 15] developed and revealed the rockburst mechanism based on the analyses of in situ stress and disturbance energy caused by mining activities. On the basis of the source and damage mechanisms, Ortlepp and Stacey [16] classified rockburst into strainburst, buckling, ejection, and collapsed arch schematic. From the triggering mechanism, rockbursts can be further divided into remotely triggered rockburst and self-initiated rockburst [17]. According to their occurring time and location of rockburst, it can be divided into immediate rockburst and time-delayed rockburst [18]. On the other hand, the mechanism of rockburst was explained by rock mechanics tests [19], such as uniaxial compression [20], unloading uniaxial compression tests, and triaxial tests [21]. For example, Su et al. [22] investigated rockburst by true triaxial tests. Wang et al. [4] investigated the rockburst triggered by hard rock fragmentations and pointed out that the rockburst triggered by pick penetration involved three progressive steps: surface slabbing, rapid ejection and violent burst of chips, and final shear failure. The numerical technique has proved to be a powerful tool for studying the mechanics of underground rock [23–25]. Compared with traditional mechanical analysis, the study of rockburst mechanism by numerical simulation is more intuitive and clearer and has been widely used to solve complex rock mechanics and engineering problems. For example, Wang et al. [26] studied the mechanism of rockburst in horizontal section mining of a steeply inclined extra-thick coal seam by combining theoretical analysis with numerical simulation. Wu et al. [27] studied the rockburst mechanism of rock mass with structural planes in underground chamber excavation by means of model test and numerical simulation and further concluded that structural planes play an important effect on rockburst phenomena. Through the discrete element method, some scholars found that when more joints are encountered, the total number of rockbursts may decrease, but the rockbursts are more likely to be strong or induce collapse, causing more damage [28].

Rockburst is a very complex dynamic geological disaster phenomenon [29, 30], and its occurrence mechanism is very complex affected by a variety of factors, such as in situ stress, rock mass integrity, rock mass strength, groundwater, construction method, blasting, and so on [31]. At present, there is no unified consensus on the mechanism of rockburst in academic circles [32, 33], but some studies have shown [32, 33] that the qualitative relationship of these factors' contribution to rockburst has been relatively clear. It is generally considered that in situ stress, rock mass integrity, and rock mass strength are the internal causes of rockburst, while groundwater, construction methods, and blasting are the external causes [31]. In this case, a factor that plays a substantial role is the in situ stress. However, at present, the law and mechanism of stress rockburst incubation are not clear. The mechanism and mode of its inoculation, development, and occurrence need to be further explored and summarized. The mechanical mechanism of stress rockburst inoculation and occurrence needs to be further revealed. In this paper, the continuous-discontinuous element method (CDEM) is adopted to conduct numerical simulation on the inoculation, development, and occurrence of three stress-type rockburst proposed by Li et al. [8], reproduce its inoculation-development-occurrence process, analyze its failure, motion, and energy characteristics, and discuss its occurrence mechanism. This study can enrich the geomechanical model of rockburst and provide a certain theoretical basis for the prediction, prevention, and control of stress rockburst.

2. Method and Model

2.1. Overview of Continuous-Discontinuous Numerical Simulation Methods. GDEM is a numerical analysis software developed by the Institute of Mechanics, Chinese Academy of Sciences, which realizes the dynamic simulation of the whole process from continuous deformation to fracture motion by coupling finite and discrete element method. Its core is CDEM based on Lagrange equation. CDEM, proposed by Professor Shihai Li, is an explicit numerical method for solving highly fused meshes and particles based on the basic framework of generalized Lagrange equations. In this method, the continuum algorithm and discontinuum algorithm are coupled, and the progressive failure process of material is simulated through the fracture of the block boundary and inside block. The numerical calculation model in CDEM-BlockdyNA consists of blocks and interfaces between blocks (Figure 1(a)). In the process from continuous to discontinuous computation, the finite element algorithm is still used for the element body in the continuous state. According to the failure criterion of different interface constitutive, the stress on both sides is calculated at each time step. When the elements on both sides of the interface reach the failure criterion, the nodes are separated into independent nodes, and their structural plane springs are set after separation (Figure 1(b)). Figure 1(c) shows the spring model at the interface. If the failure occurs, it can be divided into shear failure and tensile failure.

The CDEM uses Euler forward difference method to display and solve the force and velocity of nodes. Its basic control equations are shown in equations (1) and (2), as follows:

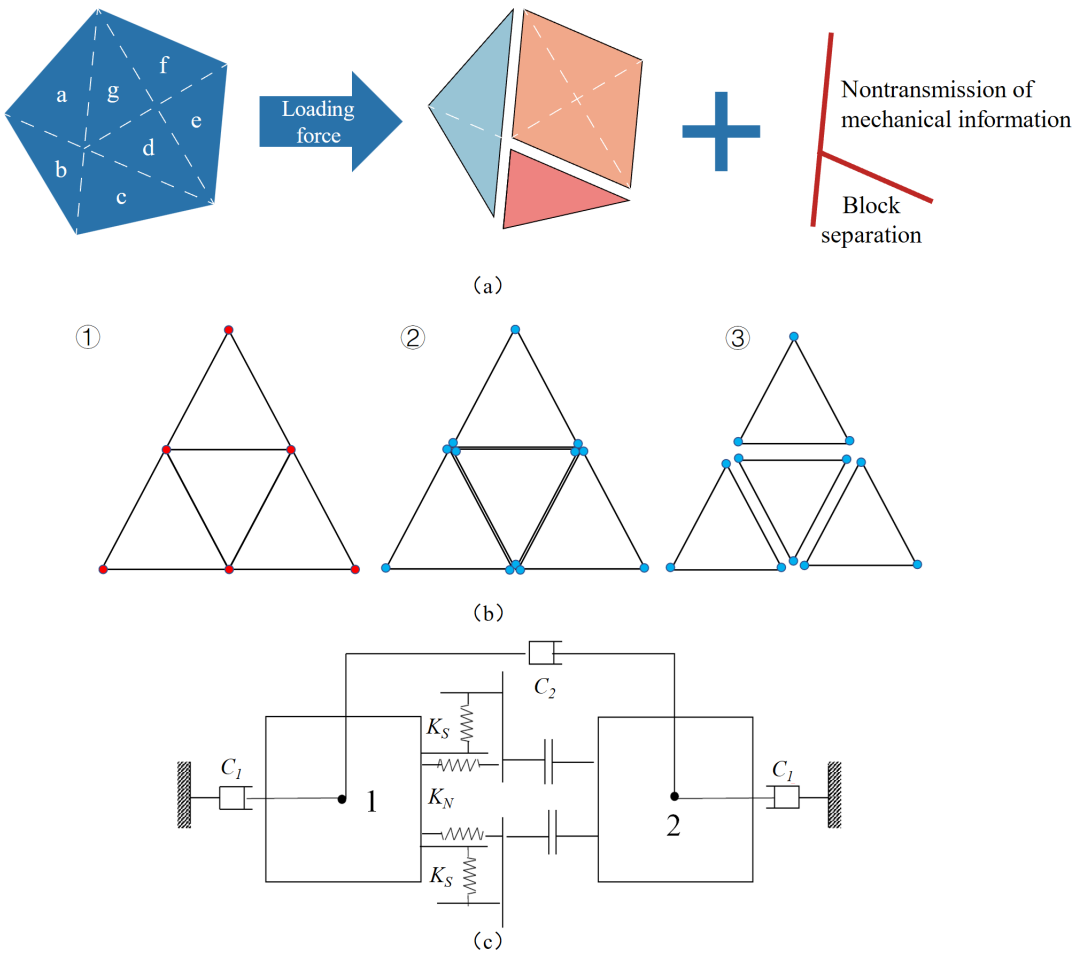

FIGURE 1: (a) Block and interface diagram of CDEM method (modified from [34]). (b) ① Continuous, ② quasicontinuous, and ③ calculate spring displacement. (c) Interfacial spring model. (k_n and k_s represent the normal and tangential contact stiffness, respectively. C_1 and C_2 represent the normal phase damping and tangential damping).

Node force:

$$m^i\ddot{\vec{u}} + c_m\dot{\vec{u}}^i = \vec{F}^E + \vec{F}_b^d + \vec{F}_b^c + \vec{F}_j^d + \vec{F}_j^c, \tag{1}$$

where $m^i\ddot{\vec{u}}$ is the inertial force, $c_m\dot{\vec{u}}^i$ is the quality damping force, $\vec{F}^E$ is the external force, $\vec{F}_b^d$ is the block deformation force, $\vec{F}_b^c$ is the block stiffness damping force, $\vec{F}_j^d$ is the interface deformation force, and $\vec{F}_j^c$ is the interface stiffness damping force.

Node displacement:

$$\left.\begin{aligned} v &= \sum_{t=0}^{T_{now}} a\Delta t \; a = F/m \\ u &= \sum_{t=0}^{T_{now}} \Delta u \; \Delta u = v\Delta t \end{aligned}\right\}, \tag{2}$$

where a is the accelerated velocity, v is the speed, Δu and u are the displacement incremental and displacement, respectively, m is the quality, and Δt is the time incremental.

The progressive failure process of geological bodies is realized by cyclic calculation. Where Δt is the time step of each iteration in the numerical calculation, and the time step should meet the convergence condition, that is, the internal force F of the system is less than the external force. Assuming that the work is done by a single spring external force, the expressions are shown in equations 3 and 4:

$$F > -F_{s1}, \tag{3}$$

$$-F_{s1} = K(F/m)\Delta t^2, \tag{4}$$

where K is the spring stiffness. As can be seen from equation (4), the iteration time step $\Delta t < \sqrt{m/k}$ is the maximum value of the iteration step, beyond which the system diverges.

This method can not only simulate the elastic, plastic, damage, and fracture process of materials under static and dynamic loads but also simulate the movement, collision, flow, and accumulation process of broken granular materials, especially suitable for the whole process simulation of progressive instability and failure of rock. It

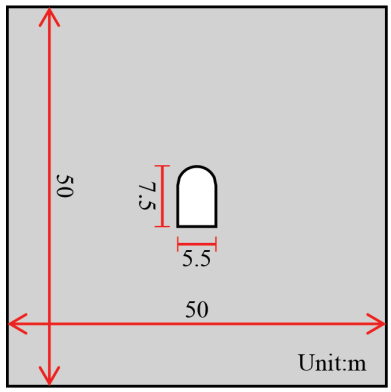

Figure 2: Dimension of model.

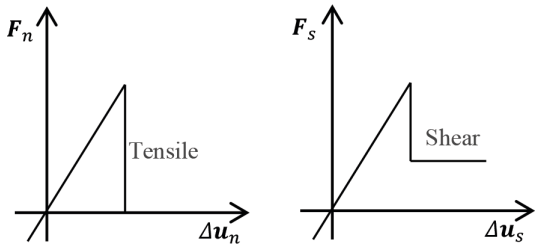

Figure 3: Virtual interface constitutive equation schematic curve. F_n and F_s are normal and tangential contact forces.

can simulate the whole process of rockburst incubation, development, and progressive failure.

2.2. Numerical Calculation Model. The numerical calculation model in this paper is selected from the auxiliary diversion tunnel of Jinping II Hydropower Station on Yalong River, Sichuan Province. The maximum measured principal stress of the auxiliary hole is 42 MPa, located at pile number 3+005 m. The tunnel has frequent rockbursts, so this tunnel is selected as the numerical simulation prototype. In general, the influence range of hard rock tunnel excavation is three to five times of tunnel diameter. Therefore, the size of this numerical calculation model is 50 × 50 m (detailed size is shown in Figure 2). As the main research focus of this paper is the inoculation-development-occurrence mechanism of stress-type rockburst, the tunnel shape selected for numerical simulation in this paper is the same shape.

Most rockbursts occur in hard brittle rock with good integrity and high strength. The rockburst in the diversion tunnel of Jinping II Hydropower Station occurred in marble, which is a hard and brittle material with high strength. Therefore, the linear elastic constitutive model was adopted for the solid unit, and the Mohr-Coulomb brittle fracture constitutive model was adopted for the virtual interface in the numerical simulation of rockburst [34]. The constitutive diagram of the virtual interface is shown in Figure 3. When the normal force between blocks exceeds the set value, the blocks are separated from each other, and the tensile strength between blocks drops to zero. When the tangential force between blocks exceeds the set value, there will be residual strength, and when the shear action continues, the shear strength is provided by friction. The physical and mechanical parameters of each stratum are shown in Table 1.

Table 1: Physical and mechanical parameters of stratum.

Stratum	ρ (g/cm^3)	σ_c (MPa)	σ_t (MPa)	C (MPa)	E (GPa)	μ
Striped mica marble	2.77	105	5.5	1.56	30	0.23
Medium-thick layer of marble	2.72	115	6.0	1.65	35	0.24
Medium-thin layer of marble	2.65	75	4.0	0.78	20	0.25
Thick-layered marble	2.80	115	5.8	1.70	37	0.22
Medium-bedded medium-fine sandstone	2.78	115	3.5	1.45	37	0.19
Interbedded sand slate	2.72	90	2.7	0.34	27	0.26

ρ: density; σ_c: uniaxial compressive strength; σ_t: tensile strength; C: cohesion; E: modulus of elasticity; μ: Poisson's ratio.

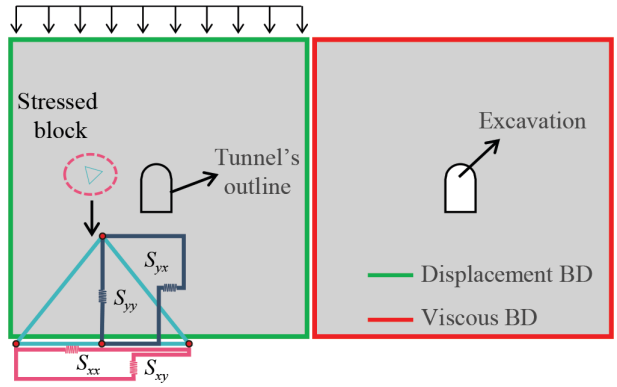

Figure 4: Schematic of the numerical simulation calculation process. "BD" is the short for boundary. The upper overburden is added in the form of a uniformly distributed load. The stress of the block is added according to normal stress and shear stress.

The numerical calculation steps are generally divided into two steps (Figure 4). (1) Elastoplastic calculation: apply displacement constraints to the left, right, and lower boundaries of the model, apply stress constraints to the upper part of the model, apply vertical uniform load to the upper rock mass of the model, then apply triaxial normal stress and shear stress to each block to simulate the structural stress, and perform elastoplastic calculation. When the unbalance rate reaches 1e−5, the next stage is calculated. (2) Dynamic calculation: the displacement and velocity generated in the calculation in the previous elastoplastic calculation stage are cleared, and the displacement constraint and stress boundary of the outer boundary

Figure 5: Tensile cracking and spalling type of rockburst. (a) Schematic diagram of rockburst patterns. (b) Typical filed image taken from the tunnel. (c) Simulated spalling type of rockburst according to field conditions.

of the model are changed into viscous boundary conditions. By setting the tunnel part as an empty element, the dynamic calculation of tunnel excavation is simulated.

3. Numerical Simulation and Analysis of Stress-Type Rockburst

3.1. Tensile Cracking and Spalling Type of Rockburst. The cacking and spalling type rockburst is characterized by sheet and plate-like spallation [8], generally without ejection, and the thickness of a single layer is 5–10 cm (Figure 5). Most of the fracture surface is straight, visible conch-shaped radial pattern. The final results of the numerical calculation are shown in Figure 5(c). It shows that the rockburst failure mainly manifests as the surface rock spalling of the left wall.

Figure 6 shows four stages of crack initiation, propagation, transfixion, and failure for rock mass. After excavation, cracks first appear near the side wall, and there is no obvious difference between the left and right side walls. However, it can be seen from Figure 6(b) that due to the preset microcracks on the left wall, the surface microcracks expand more regularly and are connected to form local failure. At this time, the crack propagation on the right side is irregular, and the failure of surrounding rock extends from the surface to the depth along the radial direction. Within 50 ms, the surrounding rock has completed the process from crack initiation to a small amount of flake blocks spalling to the surface, which can be considered as a sudden failure. From the failure process of surrounding rock, it is obvious that the rock mass failure reflects the dynamic process of "stripping first and then falling," and the spalling rock mass is flake, and the fracture surface is relatively straight. The final numerical results are consistent with the actual rockburst failure phenomenon, which shows the rationality and reliability of the numerical results.

Figures 7(a)–7(d) show the stress characteristics in each stage of tensile cracking and spalling-type rockburst. According to Figure 7, after excavation, stress redistribution occurred in a certain range, and horizontal tensile stress was first generated near the tunnel wall. With the redistribution of stress, the horizontal tensile stress gradually extends to the deep radial direction. In the whole process of stress redistribution, the horizontal tensile stress mainly exists on both sides of the sidewall, and the maximum tensile stress value decreases from 5.5 to 3.3 MPa.

Figure 8 shows the volume distribution of the block for tensile cracking and spalling-type rockburst. The volume is obtained by multiplying the area of the block by the unit width. According to Figure 8, the volume of this type of rockburst block in 0–0.25 m^3 accounts for up to 75%, and the tensile cracking and spalling-type rockburst mostly occurs in the form of gradual spallation of small blocks, which conforms to the characteristics of tensile cracking and spalling-type rockburst.

In the dynamic failure process of rockburst, part of the energy will be converted into the kinetic energy of the failure block so that it can obtain the initial motion speed. Figure 9 shows the horizontal velocity characteristics of measuring points on left wall A, B, C, and D and right wall. Under the action of horizontal tensile stress, this part of the rock mass has a tendency to move toward the surface. According to the velocity characteristics of measuring point A to point D in Figure 9, the rock mass that is closer to the surface has the tendency to move toward the surface first, indicating that rock failure develops gradually from the surface to the inside. The measuring point A is set in the surface layer of the left wall. Due to the existence of the preset microcracks, under the action of stress, it quickly penetrates, and the process of breaking through and leaving the parent body is completed in a very short time. The velocity of these blocks gradually decreases after they are separated. In this process, the average velocity of rockburst blocks is about 1 m/s, the ejection velocity of some small particles can reach 2–3 m/s, and the horizontal distance

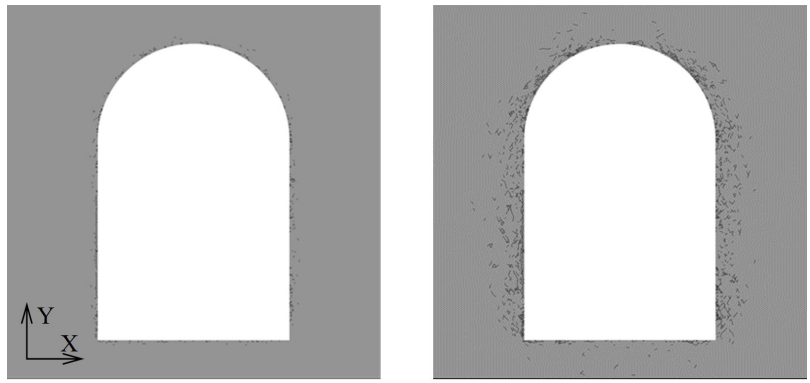

t = 0.327 ms t = 2.27 ms

t = 50 ms t = 1000 ms

FIGURE 6: Crack propagation process of tensile cracking and spalling-type rockburst.

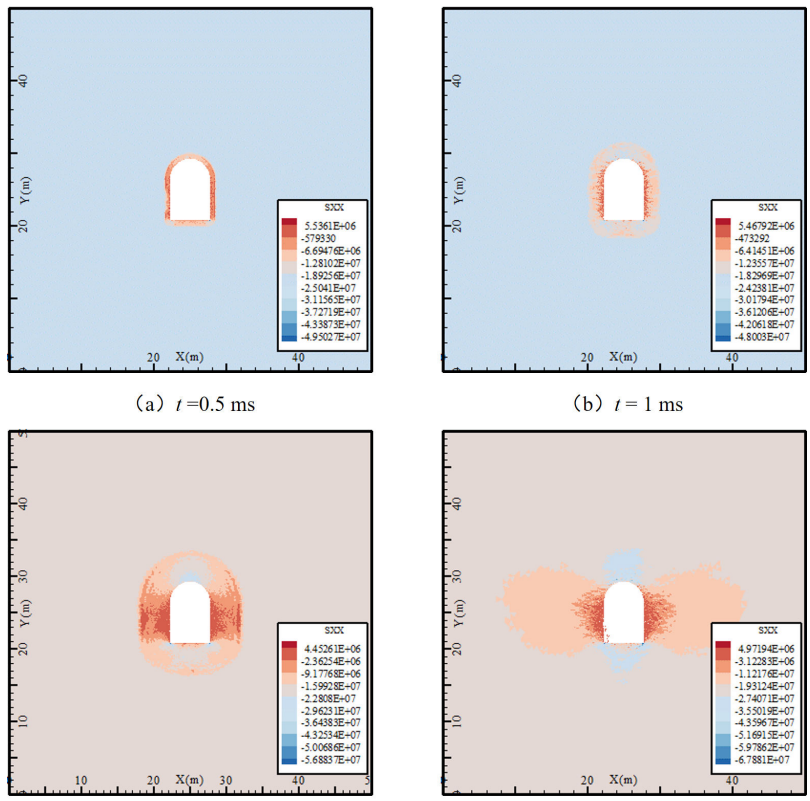

(a) t =0.5 ms (b) t = 1 ms

(c) t = 100 ms (d) t = 1000 ms

FIGURE 7: Stress change characteristics of tensile cracking and spalling-type rockburst (unit: Pa).

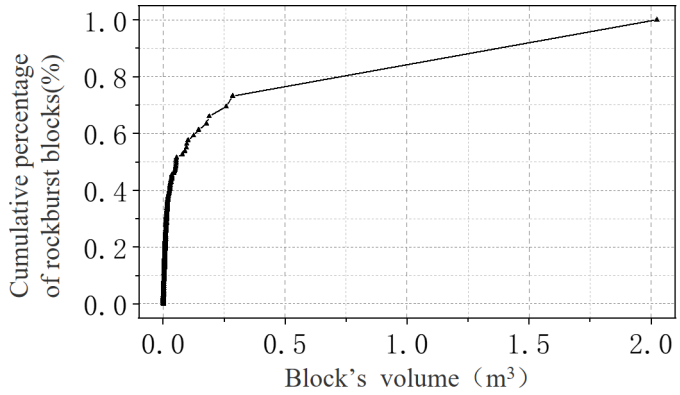

FIGURE 8: Blocks volume distribution of tensile cracking and spalling-type rockburst.

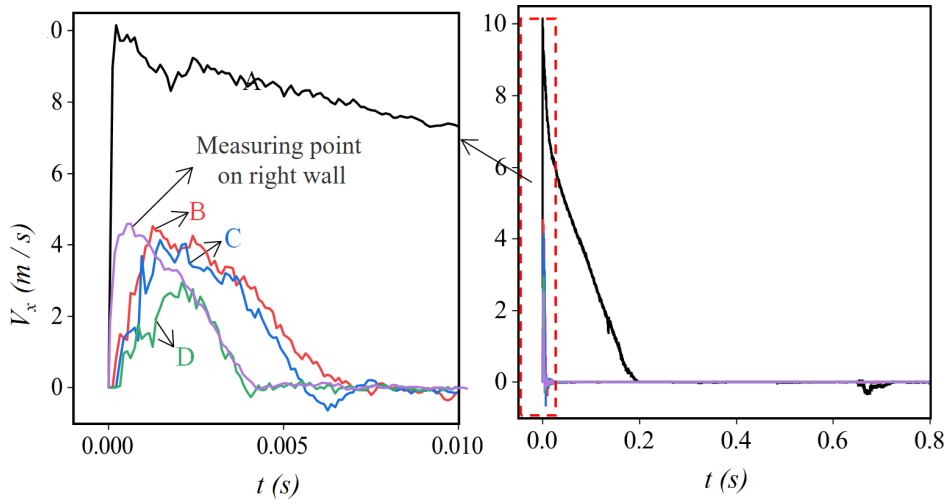

FIGURE 9: Time- history diagram of measuring points velocity of tensile cracking and spalling-type rockburst. *Vx* represents the horizontal direction, and the left diagram is a partially enlarged diagram of 0–0.01 seconds in the time-history curve.

of the whole rockburst blocks is less than 1 m. Under the action of the elastic energy released by the rock mass, the measuring points B, C, and D have a tendency to move toward the surface. However, because there is no initial preset crack, the energy is mainly used to break the rock mass, and the horizontal displacement distance is less than 1 cm.

After the shear, the horizontal velocity of the rockburst block decreases rapidly, and the movement form of the spalling block is mainly vertical falling. Figure 10 shows velocity variation in horizontal direction. Under the action of horizontal stress, the block has a tendency to move toward the surface. Due to the existence of preset cracks, rock mass cracks near the tunnel wall on the left side of the wall are the first to penetrate. Under the action of horizontal stress, the instantaneous velocity of rock mass is much higher than that of other parts. Due to the good integrity of the right wall, the rock mass has the same movement trend within a certain range of shallow layer, but most of the energy is used for rock mass to produce fracture, which is consumed by relative movement with surrounding rock mass, and the speed decreases to zero. Most of the kinetic energy of the rock mass on the left wall is used for shearing out, and the speed decreases rapidly after shearing out.

Figure 11 shows the energy variation curve in the system. Due to the existence of high in situ stress, a certain amount of elastic strain energy is accumulated in the initial stage of the system. After excavation, the elastic strain energy in the rock mass is released rapidly, causing rock mass breakage. According to Figure 11, the release of elastic energy of the system is very rapid. Only a small part of the released elastic strain energy is converted into the kinetic energy of the block. The volume of the spalling block is about 0.3 m^3 (thickness is 1), and the maximum ejection velocity of the block is taken as the movement velocity of the spalling block. It is easy to know that the maximum kinetic energy of the moving block is less than 3.64 KJ. The kinetic energy of the system is close to 500 KJ, so the kinetic energy of the block is much less than the total kinetic energy of the system. Due to the good integrity of the surrounding rock, the kinetic energy generated by the release of elastic strain energy in the system is mainly used for breaking rock mass, and only a small part of the released elastic strain energy is used for ejection energy of

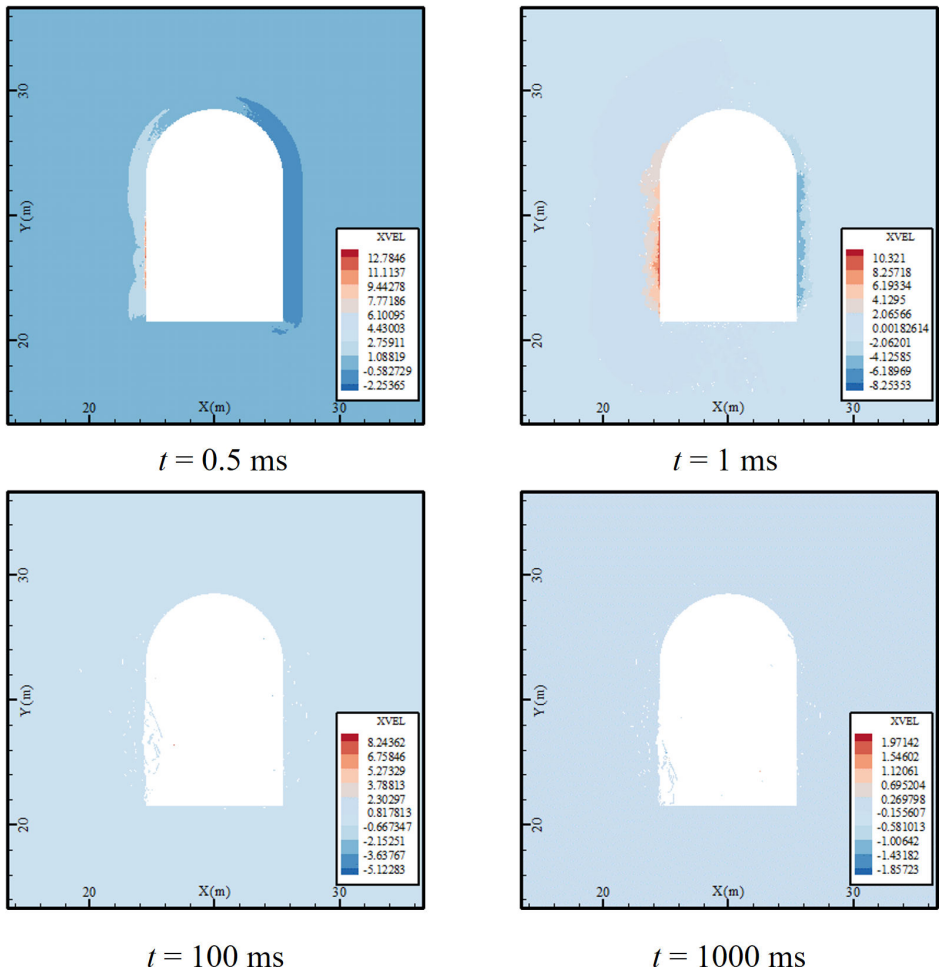

Figure 10: Horizontal velocity of tensile cracking and spalling-type rockburst (unit: m/s).

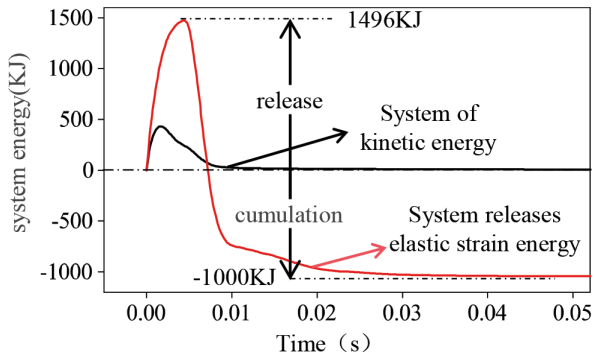

Figure 11: Energy variation curves of tensile cracking and spalling-type rockburst.

the block. After the elastic strain energy is released, a part of the elastic strain energy accumulates and continues to be stored in the rock mass in a series of stress adjustment processes. The peak value of elastic strain energy released by the system is 1500 KJ, and about 1000 KJ is finally accumulated. The energy in the whole process is lost, and the dissipated energy is mainly used for broken rock mass.

The occurrence of tensile cracking and spalling-type rockburst is the result of tensile stress. The relative motion between rock masses caused by stress difference is the cause of local shear failure. The analysis of the failure characteristics of the surrounding rock mass shows that this kind of rockburst is mainly tensile failure, which is consistent with the tensile failure in the actual case. After excavation unloading, the stress response of rock mass gradually expands inward from the cave wall, and the vertical stress of rock mass in a certain range at the side wall decreases from unloading, showing a relaxed state. However, the stress of the rock mass slightly away from the cave wall increases to some extent after unloading. The block in the damaged area has a certain compressive stress value. It can be seen that this part of the damaged rock mass is not completely destroyed and still has bearing capacity. The spalling accumulation range is within 1 m at the foot of the wall, and the ejection speed of the block is small, which is less harmful. The stress concentration area is within 2 m of the cave wall. Because the stress concentration degree does not exceed the compressive strength of the rock mass, the rock mass in the damaged area does not have a penetrating damage area, and the whole rock mass is in a mosaic state, which has a certain bearing capacity. Therefore, although the horizontal stress produced by the stress concentration area acts, it can still maintain

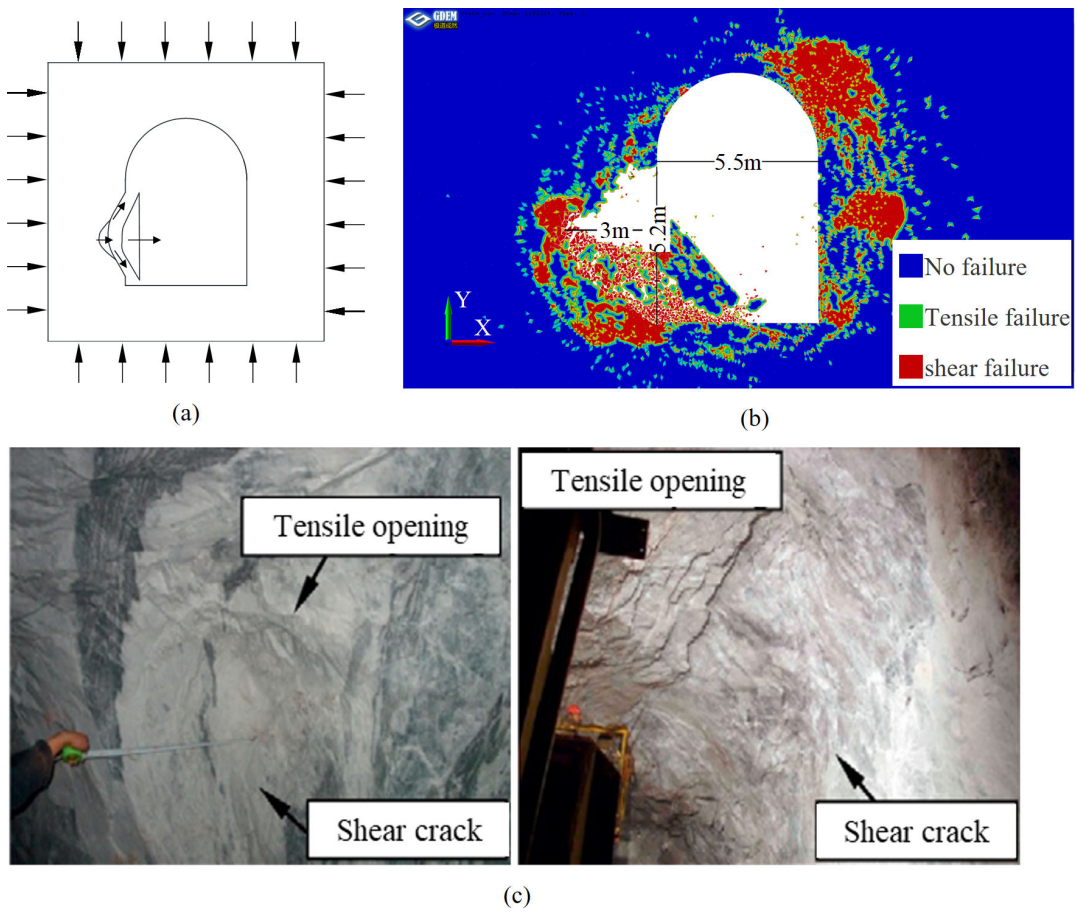

Figure 12: Arc shearing and bursting type of rockburst. (a) Schematic diagram of rockburst patterns. (b) Typical filed image taken from the tunnel. (c) Simulated arc shearing and bursting type of rockburst according to field conditions.

the overall stable state. The release of the elastic energy of the system is the cause of the kinetic energy, and the kinetic energy of the system is mainly used to overcome the linking force (cohesion, friction, etc.) between blocks. The ejection kinetic energy of rockburst blocks is far less than the kinetic energy generated by the system. The elastic strain energy released by the system will eventually be restored in the rock mass in the process of system stress adjustment, but the energy loss in the whole process is also very obvious (about 1/3), and the lost energy is mainly used for rock mass damage and unrecoverable deformation. The mechanism of the inoculation-development-occurrence process of tensile cracking and spalling-type rockburst is: sporadic tensile crack → tensile crack penetration, accompanied by a small amount of shear failure → multiple tensile fracture areas connected → port shearing, and rockburst occurs.

3.2. Arc Shearing and Bursting Type of Rockburst. Arc shearing and bursting-type rockbursts are mostly grades II–III rockbursts, which are relatively strong or intense. The dome-shaped shear-burst rockburst is mostly grades II–III rockburst, which is relatively strong or intense. The overall shape of the crater is dome-shaped (Figure 12), with the deepest horizontal direction of up to 3 m and a length of about 5.2 m. According to Figure 12(c), rock mass failure is mainly dominated by shear failure. The rock mass in the corner experienced strong shear in the process of burst block shear failure, and the block in this area was completely broken. Although the rock mass at the bottom of the crater was not carried out by the movement of the rockburst block, serious damage occurred in the shear process, and it was loose accumulation. The rock mass integrity of the upper part of the pit is still good, and the damage area is discontinuous and relatively stable. The right wall rock also has some damage, and the damage radius is close to the damage radius on the left. Because the integrity of the surrounding rock is good and the elastic strain energy released by the system is consumed due to the failure of rock mass on the left side, the internal damage of rock mass is not dispersed and continuous. Arc shearing and bursting type rockburst motion are characterized by continuous burst and rapidly extend to the depth of surrounding rock, and then the blocks are thrown out, with a sweep depth of about 3.5 m. The shape of the rockburst block is massive and granular, mainly shear failure, with a small amount of tensile shear failure. The main phenomenon of numerical simulation is consistent with the actual arc shearing and bursting type rockburst.

Figure 13 shows the whole failure process of arc shearing and bursting-type rockburst. Under the action of stress, the

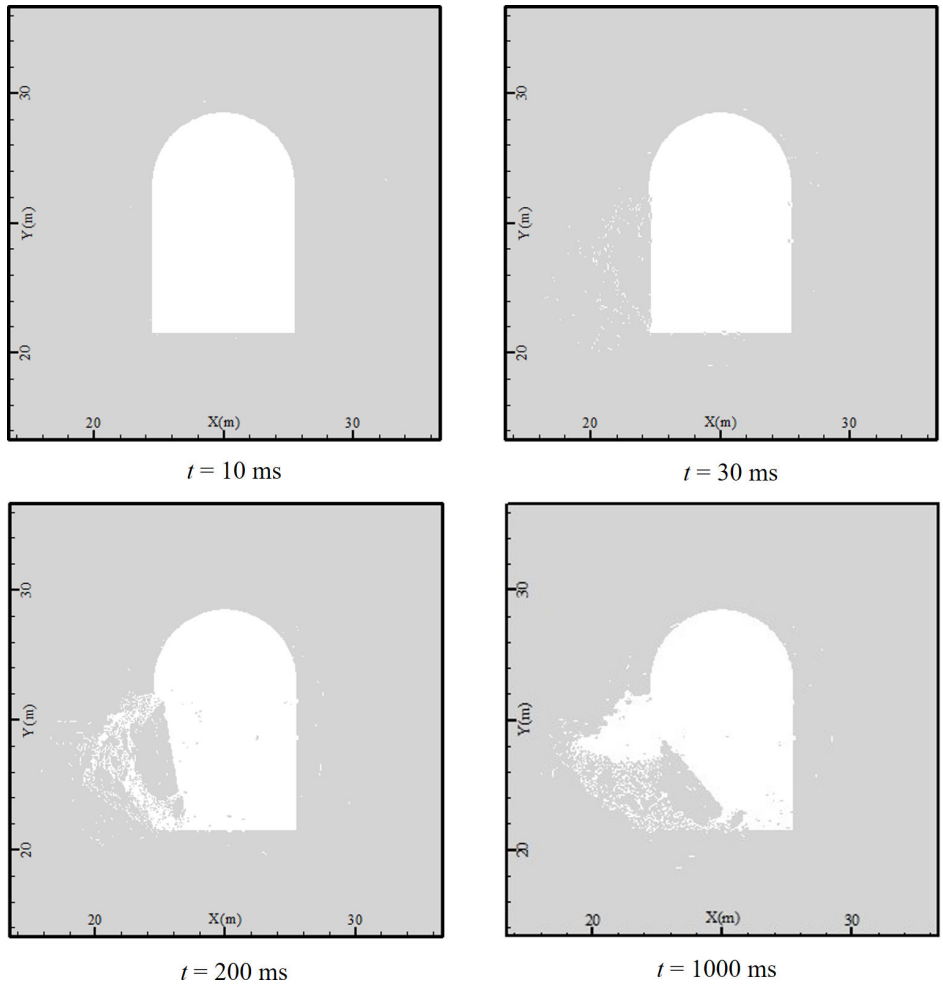

Figure 13: The failure process of arc shearing and bursting-type rockburst.

microcracks in the rock expand, and finally, the through cracks are formed. The residual elastic strain energy in the rock is converted into kinetic energy, which causes the rockburst block to move parabolically. In the failure process of shearing and bursting-type rockburst, not only large blocks are thrown out (as shown in Figures 13(b) and 13(c)) but also the rock mass on the left side of the thrown block breaks away from the surrounding rock under stress, resulting in progressive failure, and the rock mass fragmentation gradually develops to the deep part.

After excavation, the stress decreases in a certain area of the tunnel (Figure 14(a)). At the same time, the horizontal tensile stress of 5–10 MPa appears on both sides of the side wall, and the vertical stress shows a small stress concentration. With the stress adjustment and extending to the deep part, the rock mass of the left side wall is easier to break due to the preset cracks, and the stress in the broken area decreases rapidly and continues to move to the deep part, while the horizontal tensile stress also decreases gradually (Figure 14(b)). About 3 m away from the left wall, a concentrated area of compressive stress gradually formed, with a magnitude of 60–80 MPa, and a small part of the maximum compressive stress reached 98 MPa. According to Figure 14(c), the crack extends to about 3 m away from the left side wall, stopping further deep propagation to the left, and its maximum stress value is also reduced from 100 to about 90 MPa. After that, the system showed a stable state.

Figure 15 is the volume distribution diagram of the shear-explosion rockburst block, and the volume is obtained by multiplying the area of the block by the unit width. According to Figure 15, the volume of the block is 0–0.5 m^3, accounting for 70%, of which the maximum volume is 4 m^3. It can be considered that the shear-burst rockburst produced strong shear action in the process of gestation-development rockburst. The rock mass around the blast pit is sheared and becomes very broken.

Force is what changes the state of motion of an object, causing it to accelerate from rest to motion. After excavation, the release of elastic energy damages the rock mass and then destroys it. Failure is the result of relative displacement among the components of the system. Figure 16 shows the velocity time-history curves of seven measuring points on the left wall. According to Figure 16, the speed change rules of No.1, No.2, and No.3 measuring points located on the largest blasting block are similar. As the No.3 measur-

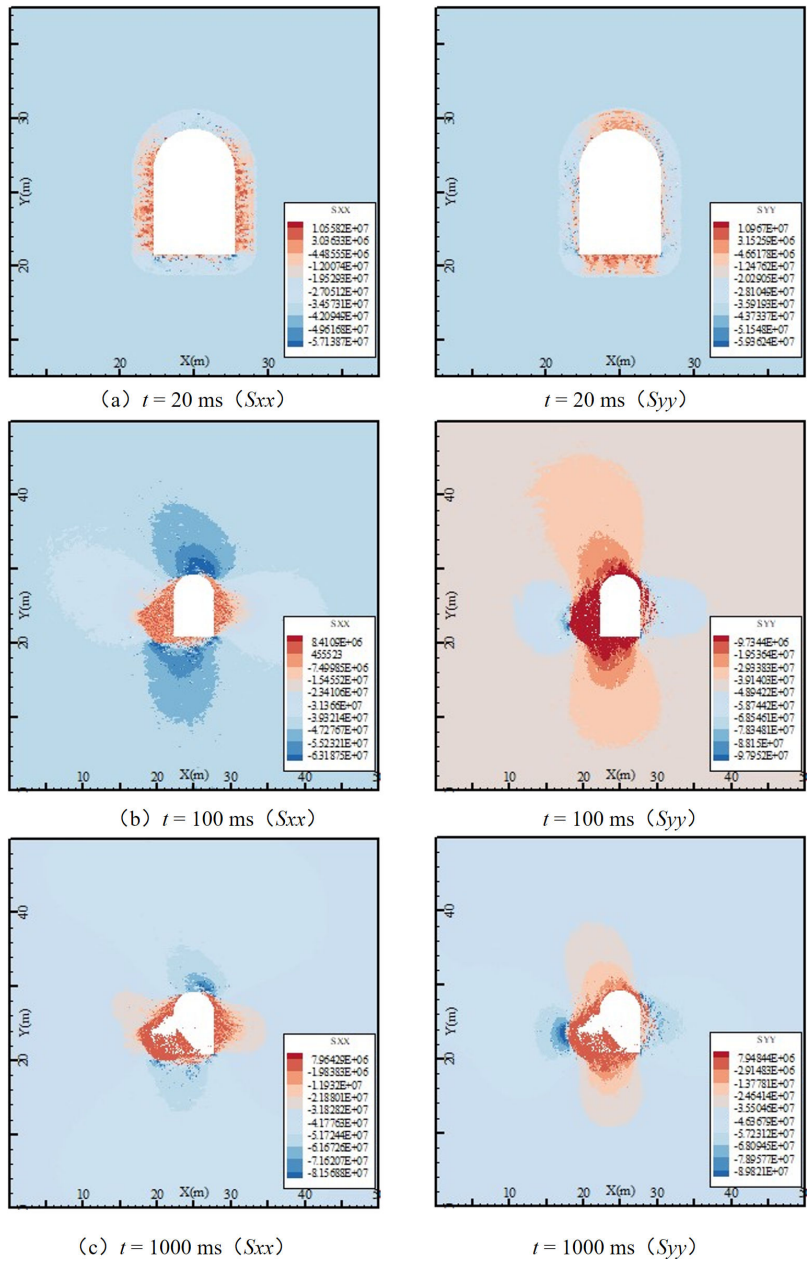

FIGURE 14: Stress change characteristics of arc shearing and bursting-type rockburst (unit: Pa). Sxx represents the normal stress in *x*-direction. Syy represents the normal stress in *y*-direction.

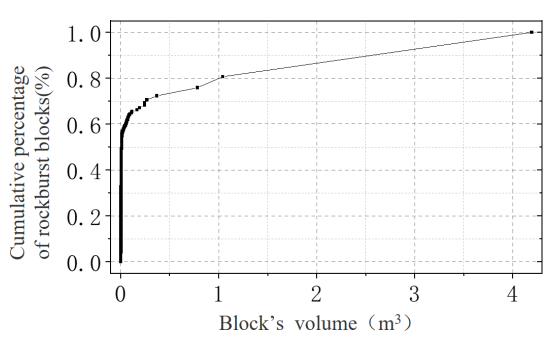

FIGURE 15: Blocks volume distribution of arc shearing and bursting-type rockburst.

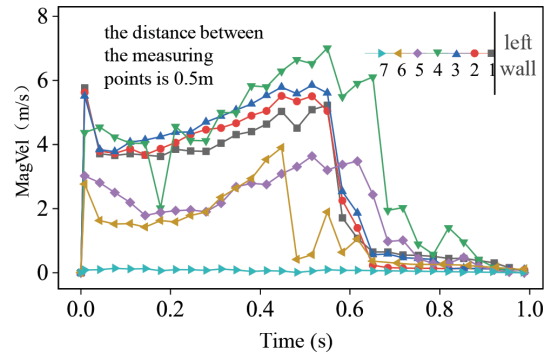

FIGURE 16: Time-history diagram of measuring points velocity of arc shearing and bursting-type rockburst.

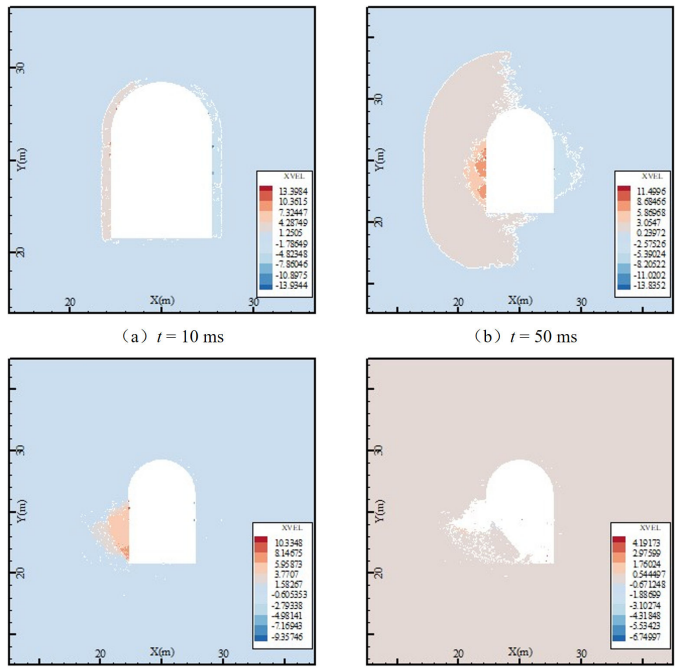

FIGURE 17: Horizontal velocity of arc shearing and bursting-type rockburst (unit: m/s).

ing point is closest to the rockburst surface, its speed is higher than that of No.1 measuring point at the side wall, which "pushes" the block outward, and the final speed is basically the same. No.4, No.5, and No.6 measuring points have the same movement trend. At the beginning, due to the outward expansion trend of the system, the initial velocity is obtained, but then the rock mass is damaged and energy is dissipated, so the velocity slowly decreases. Due to the explosion of the rock mass on the right side of No.4 measuring point, a new surface was formed in this part, and the originally damaged rock mass showed progressive failure under the action of stress concentration. According to the No.7 measuring point, the rock mass about 3.5 m away from the side wall hardly moves and is in a relatively stable state.

Figure 17 is the horizontal velocity of arc shearing and bursting-type rockburst. After excavation, the movement trends of the left and right side walls are similar in scope and velocity (Figure 17(a)). However, in the process of stress adjustment, due to the existence of the preset crack on the left side, the movement of the block on the left side wall has a larger expansion range, and the velocity gradient is obvious (Figure 17(b)). The rock mass within a certain depth range of the right side wall has an instantaneous velocity of about 5 m/s, and the velocity in the region is average without an obvious gradient (Figure 17(b)). After stress adjustment, the rock mass is further broken, forming a continuous failure area on the left wall, and the failure block tends to be thrown horizontally (Figure 17(b)). After stress adjustment, the rock mass is further broken, forming a continuous failure area on the left wall, and the failure block tends to

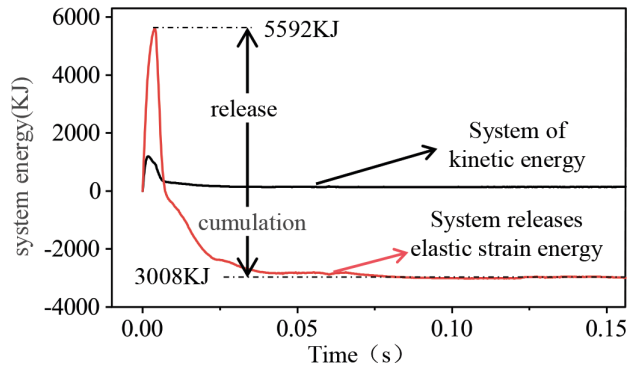

FIGURE 18: Energy variation curves of arc shearing and bursting-type rockburst.

be thrown horizontally (Figure 17(c)). Meanwhile, under the action of compressive stress, obvious compression-shear failure occurred at the left corner (Figure 17(c)). The residual energy after the rock mass is broken is converted into its kinetic energy. Finally, as shown in Figure 17(d), the block is thrown out, and finally, the whole system is in a stable state.

Figure 18 shows the variation of elastic strain energy and kinetic energy in the system. According to Figure 18, the system released 5592 KJ elastic strain energy and finally accumulated about 3008 KJ strain energy. During the whole process, 1584 KJ of energy was consumed, and the kinetic energy of the system consumed was about 1200 KJ. In the kinetic energy of the system, the ejection kinetic energy of the block, roughly calculated by the kinetic energy formula, was about 384 KJ, accounting for a relatively low proportion of the energy consumption of

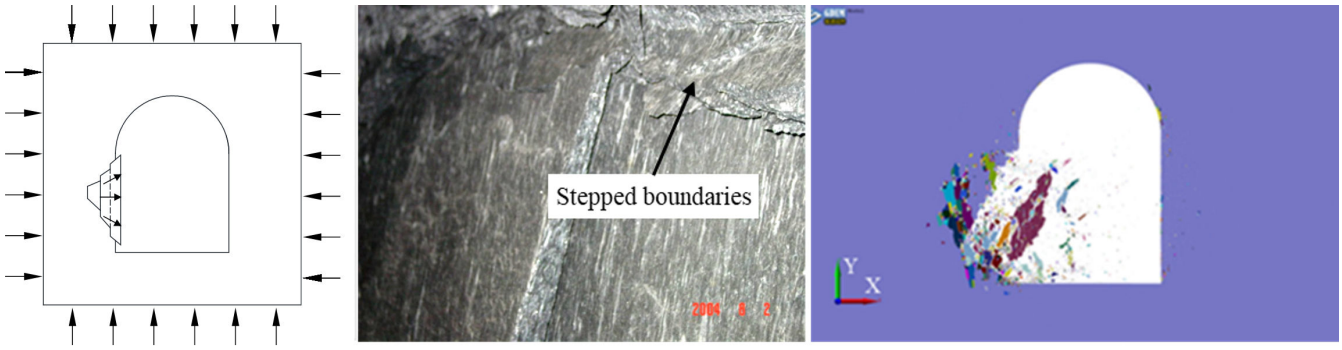

FIGURE 19: Tensile shearing and bursting type of rockburst. (a) Schematic diagram of rockburst patterns. (b) Typical filed image taken from the tunnel. (c) Simulated Tensile shearing and bursting type of rockburst according to field conditions.

the whole system. The energy consumed by the system is mainly used for broken rock mass. The release of elastic energy is not completely dissipated. Most of the energy is released, which leads to the interaction between rock masses. Because hard rock has high strength and good energy storage capacity, eventually, some energy will then accumulate in the rock in the form of elastic energy. After excavation, the stress of some rock masses in a certain area will be concentrated, and the stress of some rock masses will be reduced, although they are not completely destroyed.

Arc shearing and bursting-type rockburst is a kind of intense rockburst, and the rock mass with high ground stress and high-energy storage capacity is the necessary condition for this kind of rockburst. After excavation, the rapid release of a large amount of elastic strain energy causes the rock mass to break through, which tends to move to the near-empty surface and moves after being separated from the parent rock.

In the arc shearing and bursting-type rockburst, the rapid release of elastic energy drives rock mass destruction, and the mechanism of its inoculation-development-occurrence process is as follows: tension and shear failure appear quickly and expand inward → shear-dominated through fracture surface is formed, accompanied by a small amount of tension failure → rock mass throwing → rockburst, and the rockburst blocks produced at this time have a high degree of fragmentation.

3.3. Tensile Shearing and Bursting Type of Rockburst. The surface of tensile shearing and bursting-type rockburst is arc-like, and the pit depth is about 2 m [8]. After excavation in highly stressed rock masses, tensile cracks and tensile-shear fractures develop and progressively expand toward both sides of the free surface, resulting in a wedge burst. This type of rockburst mostly occurs in massive (relatively intact) rock masses or masses with a thick-layered structure. The affected range of rockburst is relatively extensive with a considerable amount of energy released. Moreover, substantial ejection phenomena are observed. A moderate or strong grade of rockburst occurs with largely stepped or arc-like failure plane (Figure 19).

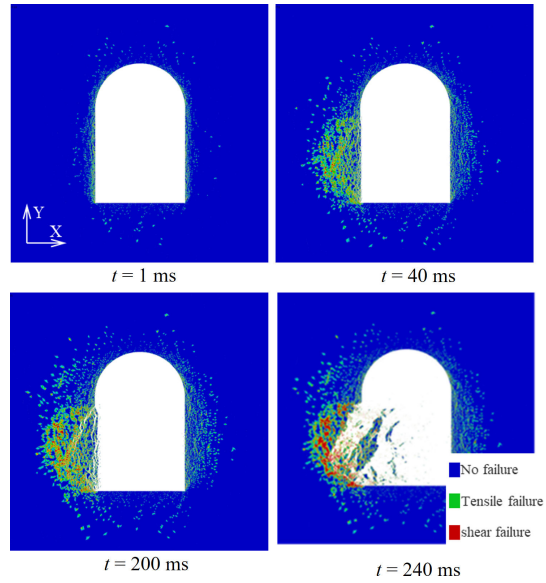

FIGURE 20: The failure process of tensile shearing and bursting-type rockburst.

Figure 20 shows the failure process of surrounding rock for tensile shearing and bursting-type rockburst. After excavation, some tension failure occurred at the side wall, and the damaged area gradually extended inward, accompanied by some shear failure. After the formation of the through failure area, shear failure occurs at the part separated from the parent rock, and the rockburst block is wedge- shaped. Because of the formation of a new surface, the rock near the explosion pit shows an outward expansion trend. In this process, some shear failure occurred in the rock mass near the blasting pit, which finally showed two kinds of mixed failure: tensile failure and shear failure. The simulation results are basically consistent with the main phenomenon of *t* tensile shearing and bursting-type rockburst in actual cases.

After the tunnel is excavated, there is a certain tensile stress near the tunnel contour at first (Figure 21(a)),

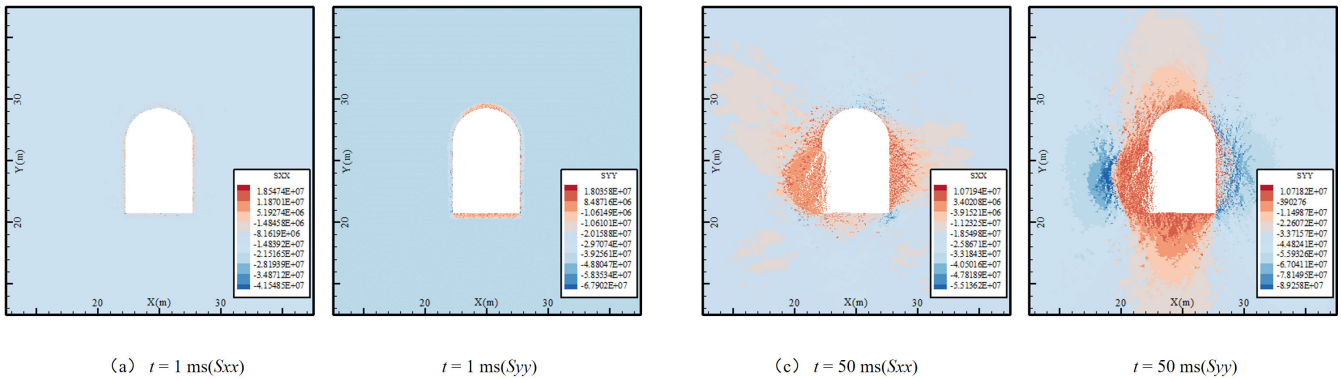

FIGURE 21: Stress change characteristics of tensile shearing and bursting-type rockburst (unit: Pa). Sxx represents the normal stress in x-direction. Syy represents the normal stress in y-direction.

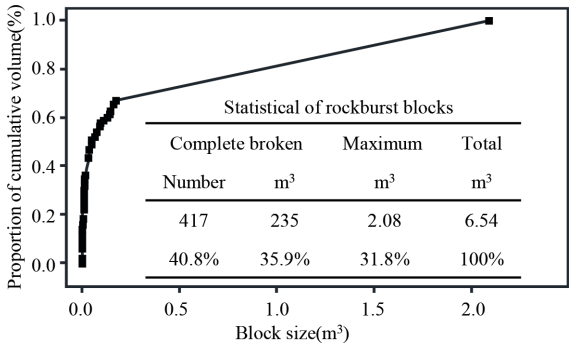

FIGURE 22: Blocks volume distribution of tensile shearing and bursting-type rockburst.

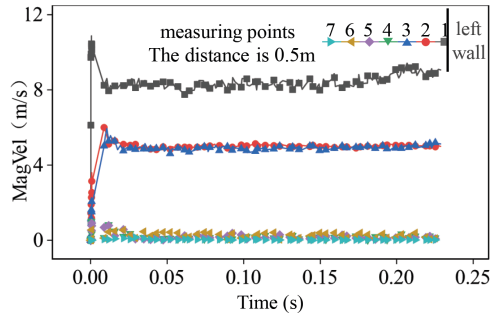

FIGURE 23: Time-history diagram of measuring points velocity of tensile shearing and bursting-type rockburst. The measuring point is located in the middle of the side wall, and the adjacent spacing is 0.5 m.

while other parts are still in the original rock stress. With the adjustment of stress, a concentrated area of vertical compressive stress appears (Figure 21(b)), and the stress value is slightly increased compared with that of the original rock, ranging from 56 to 65 MPa. At this time, the rock mass has not yet formed a connected broken area. Under the action of vertical compressive stress, the broken and penetrating area are formed (Figure 21(c)), and the stress concentration area also goes deep. After that, the rock mass failure did not further extend to the deep, and the stress concentration area also decreased, but the maximum compressive stress increased (Figure 21(d)).

According to Figure 22, rockburst blocks are 6.54 m^3 in total, of which the largest block volume is 2.08 m^3, and the proportion of completely broken blocks is only 40.8%. The proportion of completely broken blocks by blasting is small, and there are a certain number of blocks among 0.1–0.3 m^3, which indicate that the rock mass is not strongly sheared in the process of rockburst.

The velocity change of the damaged rock mass in the rockburst area and near the rockburst pit is the external manifestation of the energy change. According to Figure 23, it can be seen that the position of the moving block is about 1.5 m inward of the side wall. Rockburst

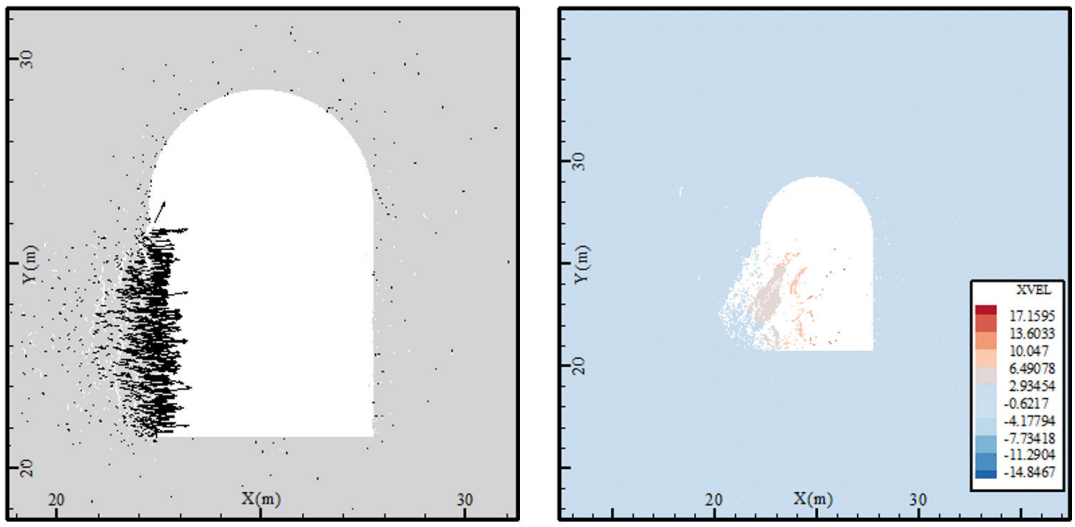

Figure 24: Horizontal velocity of tensile shearing and bursting-type rockburst (unit: m/s). (a) Vector direction (t = 50 ms) (b) The velocity in the X direction (t = 230 ms).

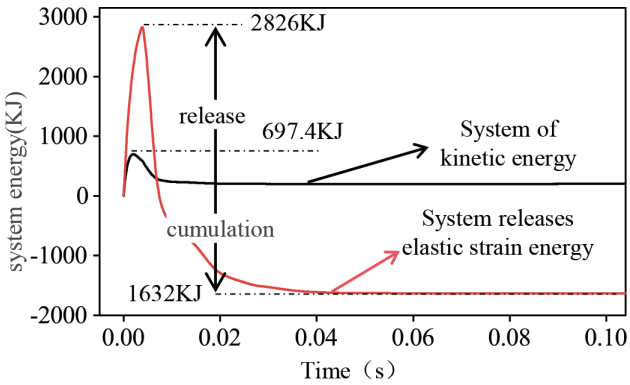

Figure 25: Energy variation curves of tensile shearing and bursting-type rockburst.

blocks have progressive characteristics from surface to deep in terms of velocity and movement time. At the side wall, small blocks or small particles of the rock mass were first ejected. Measuring point 1 was located on the small ejection block, and it was the first ejection with a velocity of about 8 m/s. Measuring points 2 and 3 are located on the largest ejection block, and their ejection time is a little later than that of Measuring point 1. On the other hand, there are slight speed fluctuations at No.4, No.5, No.6, and No.7 measuring points, which are mainly caused by rock mass damage. It can be considered that the rock mass at these four measuring points is in a stable state. It can be seen from Figure 24 that when rockburst occurs, the block mainly moves in the horizontal direction. The movement characteristics of rockburst block are as follows: there are small blocks ejected from the side wall, and the movement speed is faster than that of large blocks. The closer the initial position is to the side wall, the faster the ejection speed of rock mass is.

Figure 25 shows the energy variation characteristics of tensile shearing and bursting-type rockburst system. After excavation, the system released a total of 2826 KJ of elastic strain energy, and after stress adjustment, it reaccumulated to 1632 KJ of elastic strain energy, which consumed 1194 KJ of energy in the process. The peak value of the kinetic energy of the system is about 687.4 KJ, but after the kinetic energy of the system is stable, it still has about 209 KJ, which is the kinetic energy of the ejection block.

In conclusion, the mechanism of the inoculation-development-occurrence process of tensile shearing and bursting-type rockburst is: tension failure at the side wall → tension failure extends inward, accompanied by shear failure → tension and shear failure acting together, and through failure area formed → rockburst occurs.

4. Discussion

The characteristics of three stress-type rockbursts are compared and analyzed, and the results are shown in Figure 26. According to Figure 26, there are obvious differences in rockburst block volume, maximum block volume, and completely broken block volume. In the arc shearing and blasting-type rockburst, the damage is the strongest, the number of rock fragments is the largest, and the volume of blasting blocks is the largest. Tensile shearing and bursting type rockburst followed by these feature data, and those of tensile cracking and spalling type rockburst are in the end. At the same time, the fragmentation degree of rockburst blocks reflects the shear failure degree of rock mass in the process of deformation and failure. The stronger the shear failure, the more completely broken the blocks (loose particles). The bulk volume of tensile cracking and spalling-type rockburst is mainly distributed in (0, 0.01] m^3, and the total volume is about 0.302 m^3. The bulk volume of arc

Table 2: Statistical table of stress-type rockburst characteristic information.

Rockburst type	Movement characteristics	Affected depth (m)	Block form	Failure mode	Maximum ejection speed (m/s)	Radius of accumulation area (m)	Energy loss (KJ)	The kinetic energy peak (KJ)
Tensile cracking and spalling-type rockburst	Stripping and loosening	<0.2	Flake	Tensile cracking	8	<1 m	496	1191
Arc shearing and bursting-type rockburst	Burst and throw	3.5	Bulk and particle	Shear	11	>3 m	2584	483
Tensile shearing and bursting-type rockburst	Burst, throw, and small block ejection	1.5	Slab and loose block	Mixed failure of tension and shear	16	>4 m	1208	694

shearing and bursting-type rockburst is mainly distributed in (0, 0.5] m^3, the maximum volume is about 3.85 m^3, and the total volume is about 10.66 m^3. The volume of tensile shearing and bursting-type rockburst is mainly distributed in (0, 0.25] m^3, the maximum is about 2.08 m^3, and the total volume is about 6.54 m^3. The volume of rockburst block reflects the intensity of rockburst and the damage degree of different rockbursts.

Rockburst not only produces ejection of blocks but also damages the looseness of rock mass in a certain depth near the blasting pit. In the rockburst process, there are three failure modes: tensile failure, tension-shear mixed failure, and compression-shear mixed failure. The failure types of different rockburst modes are very different. The tensile failure is the main failure type of the tensile cracking and spalling-type rockburst, while the shear failure is the main failure type of arc shearing and bursting-type rockburst (Table 2). Meanwhile, the failure mode of surrounding rock in different areas is different. The failure process of shallow rock mass is mainly tensile failure, while the failure process of deep rock mass is tensile failure, followed by shear failure. Under the action of the mixed failure of tension and shear or mainly shear failure, the surrounding rock mass is macroscopically damaged to form a through fracture zone and then rockburst occurs. In addition, the ejection speed of individual rockburst blocks cannot fully explain the destructive ability of rockburst. In the process of rockburst, the ejection speed of large blocks is relatively slow (<6 m/s), while the ejection speed of small particles can reach 20 m/s, indicating that the peak of the ejection speed of blocks does not fully represent the intensity of rockburst. The closer the rockburst block is to the side wall, the greater its initial velocity. The ejection speed of tensile cracking and spalling-type rockburst block is less than 1 m/s. The velocity of arc shearing and bursting-type rockburst block is 2–4 m/s. The ejection speed of tensile shearing and bursting-type rockburst block is 4–8 m/s. The loss of system energy reflects the extent of rock mass destruction. The arc shearing and bursting-type rockburst energy loss is the largest, and rockburst activity is the most severe. It can be seen that the arc shearing and blasting-type rockburst

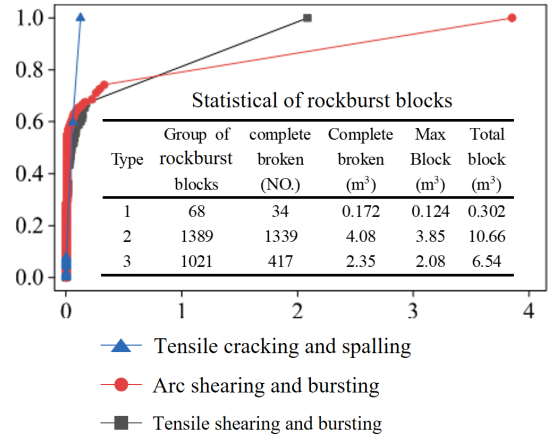

Figure 26: The characteristics of blocks for three stress-type rockburst. 1 is tensile cracking and spalling-type rockburst, 2 is arc shearing and bursting-type rockburst, and 3 is tensile shearing and bursting-type rockburst.

is the most destructive of three stress-type rockbursts, which has a great influence on the project. However, tensile cracking and spalling-type rockburst has small wave depth, little energy release, and little impact on the project.

In the process of rockburst inoculation-development-occurrence, elastic strain energy is characterized by both release and storage. The elastic strain energy release characteristics of three stress-type rockbursts are compared and analyzed, and the results are shown in Figure 27. According to Figure 27, the three types of rockbursts have experienced the process of elastic energy release and accumulation, but there are obvious differences among them. First, there is an obvious difference from the peak value of elastic energy release of the system, which shows that the peak value of elastic energy release of arc shearing and bursting-type rockburst is the largest, followed by tensile shearing and bursting-type rockburst, and finally, tensile cracking and spalling-type rockburst. According to Figure 27(b), it can be seen from the comparison of the area ratio before and after the peak of elastic strain energy release of rockburst in three modes that the ratio is inversely proportional to the rockburst destruction, and

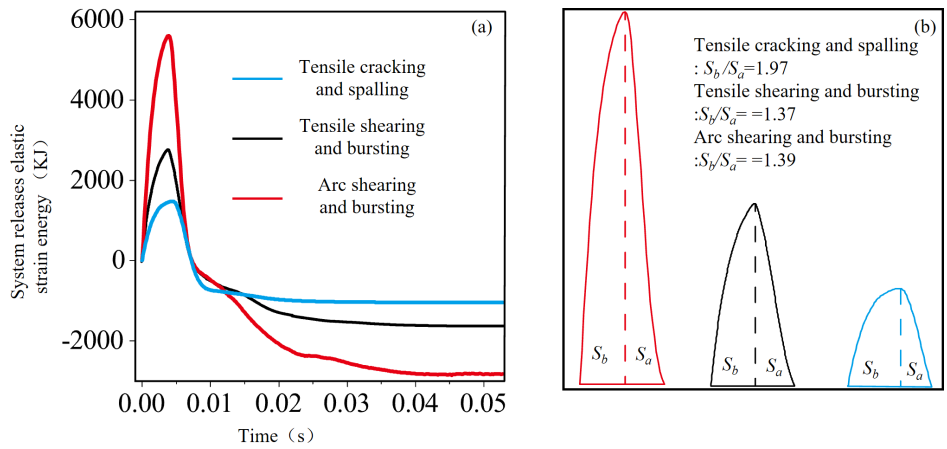

Figure 27: Comparison diagram of the kinetic energy of the system. (a) Kinetic energy of system. (b) Ratio of pre-peak area to post-peak area of energy.

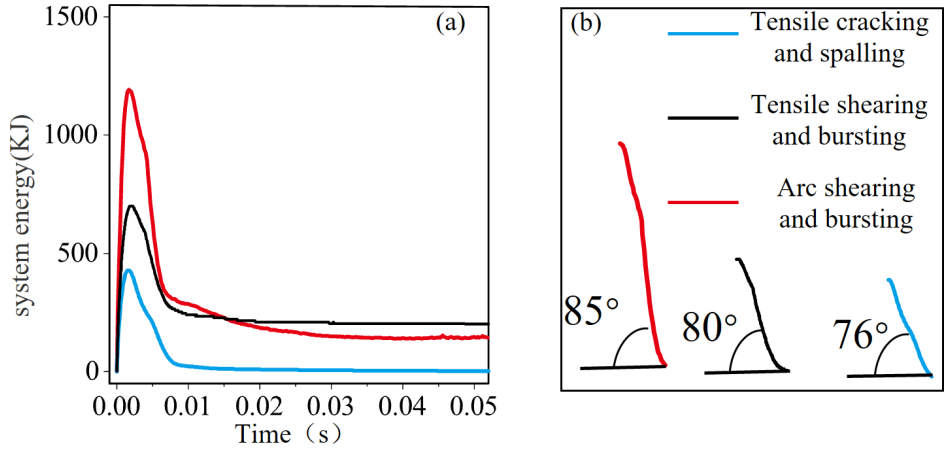

Figure 28: Comparison diagram of Kinetic energy release phase of system. (a) Kinetic energy of system. (b) System kinetic energy decline rate.

the ratio of arc shearing and bursting-type rockburst is the smallest, indicating that the process of elastic energy release and accumulation is more rapid. Generally, there is a positive correlation between the intensity of rockburst and the release of elastic strain energy. There is also a positive correlation between the energy loss and the release of elastic strain energy in the process of rockburst inoculation.

The kinetic energy changes of three stress-type rockburst systems are shown in Figure 28. The kinetic energy of the system indicates the intensity of the surrounding rock activity, with arc shearing and bursting-type rockburst > tensile shearing and bursting-type rockburst > tensile cracking and spalling-type rockburst (Figure 28(a)). The attenuation process of system kinetic energy is the process of rock kinetic energy consumption, and the reason of kinetic energy attenuation is mainly used to make rock mass produce plastic deformation, break rock mass, and the kinetic energy of broken rock mass. According to Figure 28(b), the faster kinetic energy reduction rate of the system of arc shearing and bursting-type rockburst indicates that the rock mass consumes energy faster, which can be used for the deformation and crushing of rock mass or ejection kinetic energy. It is helpful to further study the mechanism of rockburst by analyzing the proportion of each consumed energy to deeply study the law of energy change during rockburst.

5. Conclusions

In this paper, based on the CDEM, three stress-type rockbursts proposed by Li et al. [8] are analyzed from the view of numerical simulation. According to the numerical simulation results, the surrounding rock failure pattern, block characteristics, block ejection speed, and system energy characteristics during the inoculation-development-occurrence process of each rockburst are analyzed, and the following conclusions are drawn:

(1) CDEM is used to simulate rockburst, which not only shows the whole process of rock mass breakage, block ejection, crater formation, and accumulation of rockburst blocks but also monitors the change of surrounding rock failure mode, stress, velocity, and system energy change characteristics in the process

of rockburst. The numerical simulation results are in good agreement with the actual rockburst, which indicates that CDEM can be used to analyze the dynamic failure process of rockburst.

(2) The total volume and particle size of different types of rockburst blocks are quite different, which are mainly affected by stress state and geological structure. In the process of rockburst incubation, the stronger the shear failure of rock mass, the more completely broken blocks will be produced. For rockburst with tensile failure or tensile shear failure, the particle size distribution of rockburst blocks is relatively uniform.

(3) The ejection velocity of the small block is always higher than that of the large block during the same one rockburst simulation, and the ejection velocity of the small block is from the surface. The tensile cracking and spalling-type rockburst is a slight rockburst, which falls after stripping and almost no ejection, mainly affecting the superficial layer. The tensile shearing and bursting-type rockburst and arc shearing and bursting-type rockburst belong to a relatively strong rockburst with a relatively deep layer. For tensile shearing and bursting-type rockburst, the velocity of its large block is small, the velocity of its small block is large, and the overall ejection kinetic energy is large. The velocity of the arc shearing and bursting-type rockburst block is small, but the kinetic energy of the ejection block is large.

(4) The mechanism of the inoculation-development-occurrence process of stress-type rockburst can be summarized as follows: a small amount of tensile failure on the surface → shear failure → tensile failure (if it continues to extend to the deep part) → shear failure (through fracture area formed) → rockburst. The failure characteristics are as follows: shallow surface failure and mainly tensile failure. The deep failure is the mixed failure of tension and shear. When the failure depth is large, the rock failure is mainly tensile shear failure and compressive shear failure.

(5) In the process of rockburst, elastic strain energy is not only released but also accumulated. The greater the rockburst intensity, the higher the peak value of elastic strain energy released during rockburst, and the steeper the curve before the peak value of elastic strain energy. The smaller the ratio of prepeak area to postpeak area of elastic strain energy, the greater the intensity of the rockburst.

Data Availability

Data used to support the results of this study can be found in this manuscript text.

Conflicts of Interest

The authors declare that they have no known competing financial interests or personal relationships that could have appeared to influence the work reported in this paper.

Acknowledgments

This work was supported in part by the National Natural Science Foundation of China (Nos. 42130719, U19A20111, and 42107211), Opening fund of State Key Laboratory of Geohazard Prevention and Geoenvironment Protection (Chengdu University of Technology) (Nos. SKLGP2017Z001 and SKLGP2022K014), and fund of Jiangxi Provincial Department of Science and Technology (20202ACBL214016, 20224ACB204021).

References

[1] P. Li and M. Cai, "Challenges and new insights for exploitation of deep underground metal mineral resources," *Transactions of Nonferrous Metals Society of China*, vol. 31, no. 11, pp. 3478–3505, 2021.

[2] X. Li, F. Gong, M. Tao, et al., "Failure mechanism and coupled static-dynamic loading theory in deep hard rock mining: a review," *Journal of Rock Mechanics and Geotechnical Engineering*, vol. 9, no. 4, pp. 767–782, 2017.

[3] P. Małkowski and Z. Niedbalski, "A comprehensive geomechanical method for the assessment of rockburst hazards in underground mining," *International Journal of Mining Science and Technology*, vol. 30, no. 3, pp. 345–355, 2020.

[4] S. F. Wang, L. Q. Huang, and X. B. Li, "Analysis of rockburst triggered by hard rock fragmentation using a conical pick under high uniaxial stress," *Tunnelling and Underground Space Technology*, vol. 96, February, p. 103195, 2020.

[5] J. Zhou, X. B. Li, and H. S. Mitri, "Evaluation method of rockburst: state-of-the-art literature review," *Tunnelling and Underground Space Technology*, vol. 81, no. 81, pp. 632–659, 2018.

[6] F. Liu, C. A. Tang, Y. J. Zhang, and T. H. Ma, "Rockburst and microseismicity characteristics in the qinling water conveyance tunnel of the hanjiang-to-weihe river diversion project," *International Journal of Rock Mechanics and Mining Sciences*, vol. 148, December, p. 104973, 2021.

[7] R. X. Xue, Z. Z. Liang, N. W. Xu, and L. L. Dong, "Rockburst prediction and stability analysis of the access tunnel in the main powerhouse of a hydropower station based on microseismic monitoring," *International Journal of Rock Mechanics and Mining Sciences*, vol. 126, February, p. 104174, 2020.

[8] T. B. Li, C. C. Ma, M. L. Zhu, L. B. Meng, and G. Q. Chen, "Geomechanical types and mechanical analyses of rockbursts," *Engineering Geology*, vol. 222, no. 222, pp. 72–83, 2017.

[9] F. Q. Gong, S. Luo, Q. Jiang, and L. Xu, "Theoretical verification of the rationality of strain energy storage index as rockburst criterion based on linear energy storage law," *Journal of Rock Mechanics and Geotechnical Engineering*, vol. 14, no. 6, pp. 1737–1746, 2022.

[10] S. Ren, G. Yu, Y. Luo, D. Lu, and W. Cao, "Prevention and control effect of rockburst in superhigh-water backfilling mining under deep coal seam," *Lithosphere*, vol. 2022, no. Special 11, p. 1205774, 2022.

[11] W. J. Niu, X. T. Feng, and G. L. Feng, "Selection and characterization of microseismic information about rock mass failure for rockburst warning in a deep tunnel," *Engineering Failure Analysis*, vol. 131, January, 2022.

[12] S. Wang, X. Li, J. Yao, et al., "Experimental investigation of ROCK breakage by a conical pick and its application to non-explosive mechanized mining in deep hard ROCK," *International Journal of Rock Mechanics and Mining Sciences*, vol. 122, October, p. 104063, 2019.

[13] H. Feng, X. Ma, Y. Zhao, et al., "Research on the floor rockburst of panel entry under the mining influence: A case study," *Lithosphere*, vol. 2022, no. Special 11, 2022.

[14] M. F. Cai, "Prediction and prevention of rockburst in metal mines – a case study of sanshandao gold mine," *Journal of Rock Mechanics and Geotechnical Engineering*, vol. 8, no. 2, pp. 204–211, 2016.

[15] M. F. Cai, D. L. Xue, and F. H. Ren, "Current status and development strategy of metal mines," *Chinese Journal of Engineering*, vol. 41, no. 4, pp. 417–426, 2019.

[16] W. D. Ortlepp and T. R. Stacey, "Rockburst mechanisms in tunnels and shafts," *Tunnelling and Underground Space Technology*, vol. 9, no. 1, pp. 59–65, 1994.

[17] P. K. Kaiser, D. D. Tannant, and D. R. McCreath, *Canadian Rockburst Support Handbook*, Geomechanics Research Centre, Laurentian University, Sudbury, Ontario, 1996.

[18] X. T. Feng, Y. X. Xiao, G. L. Feng, et al., "Study on the development process of rockbursts," *Chinese Journal of Rock Mechanics and Engineering*, vol. 38, no. 4, pp. 649–673, 2019.

[19] L. Xu, F. Q. Gong, and Z. X. Liu, "Experiments on rockburst proneness of pre-heated granite at different temperatures: insights from energy storage, dissipation and surplus," *Journal of Rock Mechanics and Geotechnical Engineering*, vol. 14, no. 5, pp. 1343–1355, 2022.

[20] X. F. Si, L. Q. Huang, X. B. Li, F. Q. Gong, and X. L. Liu, "Mechanical properties and rockburst proneness of phyllite under uniaxial compression," *Transactions of Nonferrous Metals Society of China*, no. 31, pp. 3862–3878, 2021.

[21] R. Shirani Faradonbeh, A. Taheri, L. Ribeiro e Sousa, and M. Karakus, "Rockburst assessment in deep geotechnical conditions using true-triaxial tests and data-driven approaches," *International Journal of Rock Mechanics and Mining Sciences*, vol. 128, April, p. 104279, 2020.

[22] G. S. Su, L. H. Hu, X. T. Feng, et al., "True triaxial experimental study of rockbursts induced by ramp and cyclic dynamic disturbances," *Rock Mechanics and Rock Engineering*, no. 51, pp. 1027–1045, 2018.

[23] A. M. Starfield and P. A. Cundall, "Towards a methodology for rock mechanics modelling," *International Journal of Rock Mechanics and Mining Sciences & Geomechanics Abstracts*, vol. 25, no. 3, pp. 99–106, 1988.

[24] O. Vardar, C. G. Zhang, I. Canbulat, and B. Hebblewhite, "Numerical modelling of strength and energy release characteristics of pillar-scale coal mass," *Journal of Rock Mechanics and Geotechnical Engineering*, vol. 11, no. 5, pp. 935–943, 2019.

[25] C. C. Wei, C. G. Zhang, I. Canbulat, and W. P. Huang, "Numerical investigation into impacts of major fault on coal burst in longwall mining – a case study," *International Journal of Rock Mechanics and Mining Sciences*, vol. 147, November, p. 104907, 2021.

[26] S. Wang, A. Cao, Z. Wang, et al., "Study on mechanism of rock burst in horizontal section mining of a steeply inclined extra-thick coal seam," *Lithosphere*, vol. 2022, no. Special 11, 2022.

[27] J. Wu, X. Y. Zhang, L. Y. Yu, L. W. Zhang, and T. Wu, "Rockburst mechanism of rock mass with structural planes in underground chamber excavation," *Engineering Failure Analysis*, vol. 139, September, 2022.

[28] J. Wang, G. Chen, Y. Xiao, S. Li, Y. Chen, and Z. Qiao, "Effect of structural planes on rockburst distribution: Case study of a deep tunnel in southwest China," *Engineering Geology*, vol. 292, no. 294, p. 106250, 2021.

[29] M. Askaripour, A. Saeidi, A. Rouleau, and P. Mercier-Langevin, "Rockburst in underground excavations: a review of mechanism, classification, and prediction methods," *Underground Space*, vol. 7, no. 4, pp. 577–607, 2022.

[30] M. C. He, F. Q. Ren, and D. Q. Liu, "Rockburst mechanism research and its control," *International Journal of Mining Science and Technology*, vol. 28, no. 5, pp. 829–837, 2018.

[31] T. B. Li and X. P. Xiao, "Comprehensively integrated methods of rockburst prediction in underground engineering," *Advances in Earth Science*, vol. 23, no. 5, pp. 533–540, 2008.

[32] C. H. Dowding and C. A. Andersson, "Potential for rock bursting and slabbing in deep caverns," *Engineering Geology*, vol. 22, no. 3, pp. 265–279, 1986.

[33] Z. Q. Zhang, G. B. Shu, and H. M. Weng, "Basic analysis of conditions that cause rockburst," *Journal of Railway*, vol. 20, no. 4, pp. 83–86, 1998.

[34] C. Feng, S. H. Li, W. H. Hao, and W. Ge, "Numerical simulation for penetrating and blasting process of EPW based on CDEM," *Journal of Vibration and Shock*, vol. 36, no. 13, pp. 11–18, 2017.